Formation and stability of a two-dimensional nickel silicide on Ni(111): An Auger, LEED, STM, and high-resolution photoemission study

B. Lalmi,[1,*] C. Girardeaux,[2] A. Portavoce,[2] C. Ottaviani,[3] B. Aufray,[4] and J. Bernardini[2]
[1]*Synchrotron SOLEIL, L'Orme des Merisiers, Boite Postale 48, 91192 Saint-Aubin, France*
[2]*IM2NP (UMR 6242), CNRS, Aix-Marseille Université, Faculté des Sciences et Techniques, Campus de Saint-Jérôme, F-13397 Marseille cedex 20, France*
[3]*CNR-ISM, via Fosso del Cavaliere, 00133 Roma, Italy*
[4]*CINaM-CNRS, Campus de Luminy Case 913; 13288 Marseille cedex 09, France*
(Received 21 November 2011; revised manuscript received 10 May 2012; published 13 June 2012)

Using low-energy electron diffraction (LEED), Auger electron spectroscopy (AES), scanning tunneling microscopy (STM), and high-resolution photoelectron spectroscopy (HR-PES) techniques we have studied the annealing effect of one silicon monolayer deposited at room temperature onto a Ni (111) substrate. The variations of the Si surface concentration, recorded by AES at 300 °C and 400 °C, show at the beginning a rapid Si decrease followed by a slowing down up to a plateau equivalent to about one third of a silicon monolayer. STM images and LEED patterns, both recorded at room temperature just after annealing, reveal the formation of an ordered hexagonal superstructure of $(\sqrt{3} \times \sqrt{3})R30^\circ$ type. From these observations and from a quantitative analysis of HR-PES data, recorded before and after annealing, we propose that the $(\sqrt{3} \times \sqrt{3})R30^\circ$ superstructure corresponds to a two-dimensional Ni_2Si surface silicide.

DOI: 10.1103/PhysRevB.85.245306 PACS number(s): 68.35.bd, 73.40.Sx

I. INTRODUCTION

In the last decade, the study of growth of ultrathin films has greatly progressed. Much of the effort on this matter has mainly been devoted to the growth of two-dimensional (2D) layers with properties different from those of the bulk. Most of the works reported in the literature concern the deposition of thin metallic films on semiconductor. For low coverage this leads to formation of ordered and well defined structures. Many different combinations of metals and semiconductors have been extensively studied.[1–8]

The Ni-Si interface is a typical example of a system in which a number of surface phases appear during reactive diffusion. The initial stages of nucleation and growth of 2D and three-dimensional (3D) phases at the Ni/Si interface have been extensively studied by structural or microscopy surface techniques, such as low-energy electron diffraction (LEED), low-energy electron microscopy (LEEM), and scanning tunneling microscopy (STM).[9–12] Several 2D phases are reported to appear during the reaction of an ultrathin Ni film with a Si (111) substrate, $(\sqrt{3} \times \sqrt{3})R30^\circ$, $(\sqrt{19} \times \sqrt{19})R23.4^\circ$, and $(1 \times 1) - RC$ phases.[13–17] The last two phases are the most likely intermediate steps to epitaxial growth of 3D $NiSi_2$ onto Si (111).[18–20] On Si (001), depending on the Ni coverage and thermal annealing conditions, several nickel-silicide compounds can be formed.[21] Yoshimura *et al.*[22] have shown by STM that adsorbed Ni atoms immediately react with Si substrate forming a (2×1) 2D alloy. This reconstruction is induced by the dimerization of Si dangling bonds under the top Ni layer.[21,23,24] For Ni coverage over 0.7 monolayers (ML), $NiSi_2$ islands coexist with the (2×1) structure. For Si (111) and Si (100), when the Ni coverage exceeds 1 ML the surface morphology is always a miscellaneous combination of 3D islands and 2D structures.[16,20,21]

The bulk phase diagram of the Ni-Si system is asymmetric; indeed, whereas the solubility limit of Ni in Si is negligible, the solubility of Si in Ni is about 10% at 700 °C.[25] That means there is a possible Si diffusion in the bulk of Ni, which is not the case in the reverse system. In spite of many efforts to understand the structure and reaction kinetics for the Ni-Si system, there are only a few reports discussing the "reverse system," i.e., reaction of ultrathin silicon films onto nickel surfaces (Si/Ni). Yet, understanding of the nonequivalence between the sequences of deposition Ni/Si and Si/Ni is of great interest for the comprehension of the initial stages of Schottky barrier formation.

In the present study, we are interested in the early stages of Si adsorption and reaction onto the Ni (111) surface and, in particular, in formation of a possible ordered overlayer and/or interface structure which may be induced by thermal annealing. We examine in detail, using four surface-sensitive techniques [Auger electron spectroscopy (AES), LEED, high-resolution photoelectron spectroscopy (HR-PES), and STM], the precise composition, structure, and kinetics properties of the nickel-silicon interface formed, when one silicon monolayer is deposited onto Ni (111).

II. EXPERIMENTAL DETAILS

All experiments were carried out in ultrahigh-vacuum (UHV) conditions with a base pressure below 2×10^{-10} Torr. They were performed in two different pieces of experimental equipment. AES, LEED, and STM analysis were performed at CINaM, Marseille. Auger spectra were obtained in the derivative mode, and the data collected with a computer system allowing an easy measurement of the peak-to-peak height of the Auger signal of elements close to the surface versus annealing time (or deposition time). The LEED optics placed in the same chamber was used to follow the surface structure evolution. The STM (Omicron STM1) microscope, which is in the main chamber, was used at room temperature (RT) after annealing.

HRPES experiments were performed at the "VUV" beam line of the ELETTRA synchrotron radiation facility in Trieste,

1098-0121/2012/85(24)/245306(6) ©2012 American Physical Society

Italy. Electron distribution curves were recorded with a hemispherical energy analyzer. To study the Si_{2p} core levels, the photon energy was set to $E = 177.7$ eV. Before any experiment, whatever the technique used, the Ni (111) surface was cleaned by cycles of Ar^+ ion bombardment (5×10^{-5} Torr at 500 eV) followed by annealing at 750 °C. The sample temperature was evaluated from a thermocouple spot-welded on the sample holder very close to the crystal. The sputtering-annealing cycles were performed until a sharp (1 × 1) LEED pattern was observed. Silicon deposition was carried out in the main chamber by thermal evaporation from a silicon wafer heated by the Joule effect. The Si coverage has been estimated from the growth kinetics previously recorded at RT by AES on a Cu substrate.[26,27] On this substrate, the growth is close to a layer-by-layer mode, at least up to 5 ML. On the experimental curves, as well as on the simulated curves, the first break, which corresponds to the completion of the first ML, appears when the intensity of the Cu (60 eV) Auger signal is attenuated about 60%. On the simulation of the experimental curve, the Si ML was assumed to be a dense plane with a depth of 0.235 nm. In the present study, we supposed that the first Si ML is obtained when the same attenuation is reached in the Ni (61 eV) Auger signal.

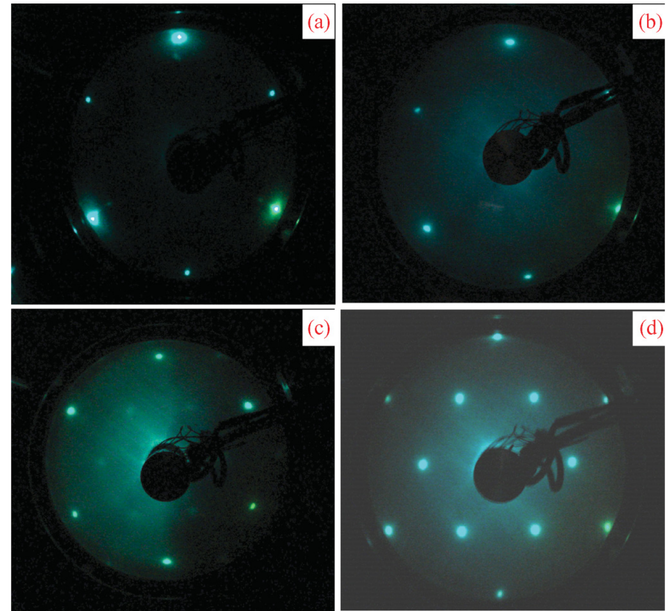

FIG. 2. (Color online) LEED patterns ($E = 64$ eV) of a Ni(111) surface (a) on bare surface; (b) after deposition of 1 Si ML; (c) after annealing at 130 °C; (d) after annealing at 400 °C.

III. RESULTS AND DISCUSSIONS

Isochronal dissolution kinetics of one silicon monolayer (1 Si ML) has been recorded in the temperature range [50 °C–650 °C] with an annealing rate of about 1.5 °C/min. During the temperature rise, the evolution of both Ni (61 eV peak) and Si (92 eV peak) Auger signals were monitored by AES measurements. Figure 1 shows the variation of the Si (92 eV) to Ni (61 eV) Auger signals' intensity ratio versus temperature. Three domains can be delimited on this curve. From room temperature up to about 130 °C (domain I), one observes a fast decrease of the Auger signals' I_{Si}/I_{Ni} ratio. This first decrease is followed by a slower decreasing (domain II) in the temperature range [130 °C–440 °C]. In the third part (domain III), the curve reaches a plateau corresponding to a I_{Si}/I_{Ni} ratio close to 0.25.

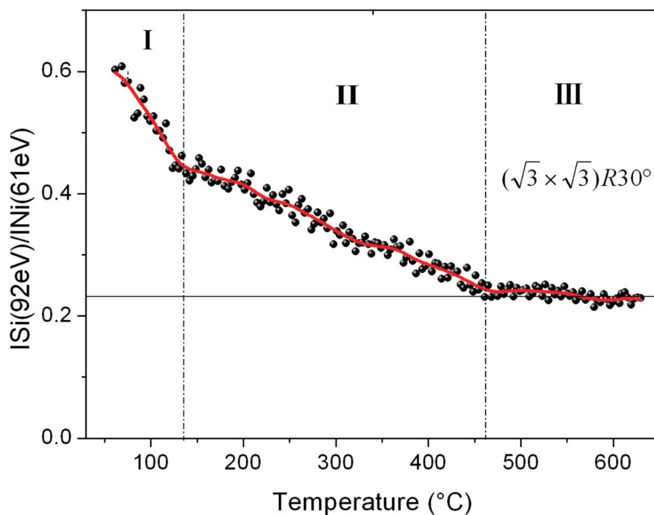

FIG. 1. (Color online) Variation of the Auger peak-to-peak intensity ratio (I_{Si}/I_{Ni}) versus temperature during isochronal dissolution of 1 Si ML deposited onto Ni(111).

During the temperature rise, the evolution of the surface structure was also followed by LEED. Figure 2(a) shows a typical sharp (1 × 1) LEED pattern ($E = 64$ eV) recorded on a clean Ni (111) face after the surface preparation. After deposition of 1 Si ML, the (1 × 1) LEED pattern is still there but the spots are more fuzzy and the background more intense which are characteristics of an unstructured deposit [Fig. 2(b)]. From about 130 °C, a $(\sqrt{3} \times \sqrt{3})R30°$ superstructure starts to appear [Fig. 2(c)] to become more and more intense and sharper as the temperature increases [Fig. 2(d)]. Note that this superstructure is observed up to 650 °C.

It is generally difficult to interpret quantitatively an isochronal dissolution kinetics because many parameters evolve with time and temperature (bulk diffusion coefficient D_b, limit of the solubility $C_{b\text{limit}}, \ldots$), mixing kinetics to thermodynamics phenomena. However, it often shows clearly the global behavior of the system, highlighting the temperature domains where interesting phenomena occur. Nevertheless the isochronal kinetics presented in Fig. 1 can be roughly understood as follows. Because the fast decrease of the I_{Si}/I_{Ni} ratio observed in the first domain ($T < 130$ °C) cannot be linked to silicon bulk dissolution (the temperature is too low) it is more likely the signature of a reaction/reorganization of the silicon ML with the very first Ni atomic layers. Such a reaction/reorganization characterized by a fast decrease in the ratio of Auger signals can correspond to (1) the formation of a thin 3D surface alloy (silicide) covering the entire surface (the superstructure observed by LEED at the end of the first domain would be the signature of a perfect epitaxy between this silicide and the Ni(111) substrate); (2) islanding of the unreacted Si deposit in equilibrium with a 2D superficial compound, which is not very likely because the Ni-Si system presents a strong tendency to form alloy and not to phase separation; or to

(3) formation of 3D silicide clusters which do not cover the entire surface in equilibrium with a superficial 2D compound (since a superstructure is observed at the end of the domain). Concerning domain II, where a slowdown is observed in the decrease of the Auger intensity ratio, two scenarios can be foreseen. The first one, based on the idea that no islanding appears at the end of the first domain [hypothesis (1) exposed previously], is the dissolution of a thin 3D surface alloy (silicide) covering the entire surface. The decrease observed in domain II corresponds then to a continuous dissolution of this thin 3D alloy (silicide) up to the formation of a 2D surface alloy (domain III) more stable than the 3D one. The second scenario would correspond to a decrease of the size of the 3D clusters up to complete dissolution (via silicon dissolution in the bulk of nickel) in equilibrium with the 2D compound forming the superstructure observed by LEED. In any case, the kinetics blocking observed in the first part of domain III can be explained by a stronger stability of the 2D compound forming the $(\sqrt{3}\times\sqrt{3})R30^\circ$ superstructure linked to the strong Si surface segregation tendency due to its lower surface energy in comparison with the nickel one.[28] Results of photoelectron spectroscopy presented later will allow us to specify the scenario.

Using the same technique (AES-LEED), isothermal dissolution kinetics have been recorded at two temperatures ($\sim$300 °C and $\sim$400 °C). The variation of Auger peak-to-peak intensity Si (92 eV) to Ni (61 eV) ratio versus time for each temperature is displayed in Figs. 3(a) and 3(b).

The LEED observations carried out at room temperature at the end of each kinetics exhibit the same sharp and well defined $(\sqrt{3}\times\sqrt{3})R30^\circ$ superstructure as observed at the end of the isochronal kinetics.

For the kinetics recorded at 300 °C, one can observe again three domains: (I) the rapid decreasing of the $I_{\mathrm{Si}}/I_{\mathrm{Ni}}$ ratio at the beginning of annealing, probably due to the reaction/reorganization previously detailed for the silicon ML with the very first Ni atomic layers, then (II), a slow continuous dissolution of a 3D compound (or 3D clusters), and (III) the kinetics blocking on the $(\sqrt{3}\times\sqrt{3})R30^\circ$ superstructure. For the kinetics recorded at 400 °C, domains I and II are probably too close (mixed) to be observed. It is interesting to note that at the end of both isothermal kinetics and at the end of isochronal kinetics, one observes the same superstructure and the same surface concentration ($I_{\mathrm{Si}}/I_{\mathrm{Ni}} \approx 0.25$). If one accepts that this ratio is mainly characteristic of Si atoms staying on the surface, it corresponds to about one third of a Si ML (two thirds have been dissolved in the nickel volume).

From isothermal dissolution kinetics it is possible to derive the order of magnitude of the bulk diffusion coefficients involved during the first part of the dissolution process. This estimation can be done easily from the time that the system uses to dissolve in the bulk around two thirds of the Si ML ($\sim$80 min at 300 °C and $\sim$30 min at 400 °C) with the assumptions that there is no evaporation as well as no island formation of silicon.

Using the relation[29–31]

$$\Delta C_s(t) = 2\, C_{b\,\mathrm{limit}} \sqrt{\frac{D_b\ t}{\pi}},$$

where D_b is the bulk diffusion coefficient, t the time to dissolve two thirds of the Si ML (ΔC_s the variation of Si amount after

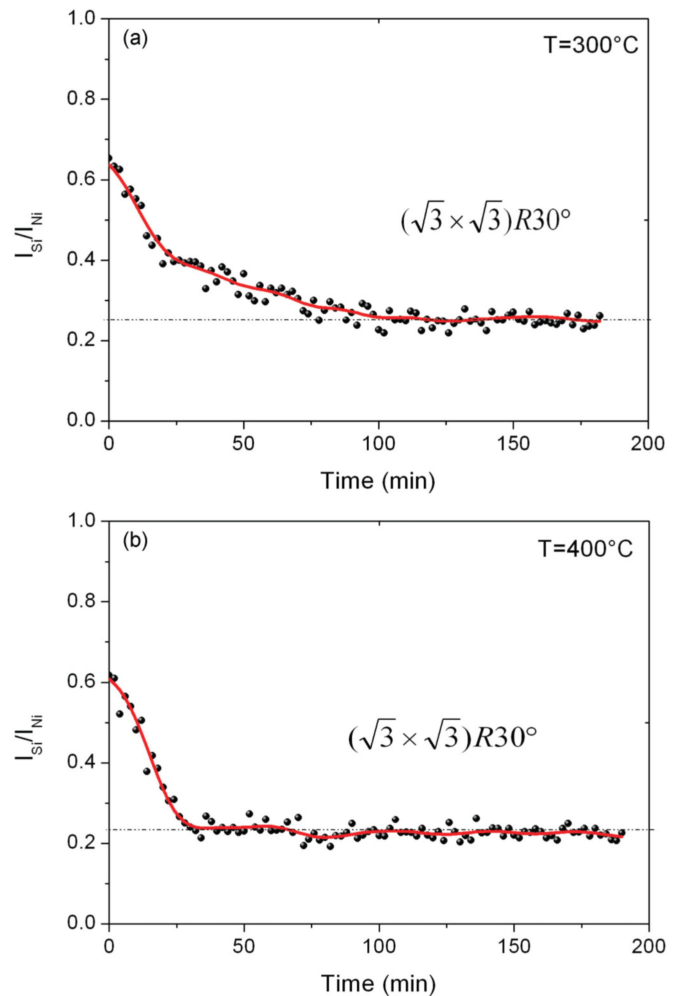

FIG. 3. (Color online) Variation of the Auger peak-to-peak intensity ratio ($I_{\mathrm{Si}}/I_{\mathrm{Ni}}$) versus time during isothermal dissolutions of 1 ML Si/Ni(111), (a) at 300 °C; (b) at 400 °C.

a time t) and $C_{b\ \mathrm{limit}}$ the limit of the solubility of Si in Ni (given by the bulk phase diagram), we have derived both bulk diffusion coefficients D_b (300 °C) $\approx 6\times10^{-18}$ cm^2 s^{-1} and D_b (400 °C) $\approx 1\times10^{-17}$ cm^2 s^{-1}. These values are very high in comparison with the values expected from extrapolation of high-temperature measurements which are, respectively, 4×10^{-24} cm^2 s^{-1} and 1×10^{-20} cm^2 s^{-1}.[32]

From this simple evaluation of the bulk diffusion coefficients we can deduce that the first parts of the kinetics are not only linked to a bulk dissolution process but also to a reaction/reorganization of Si atoms with the first Ni layers.

Note that similar kinetics behaviors have been also observed on equivalent bimetallic systems, i.e., with a tendency to order and to a strong surface segregation of the deposited element.[33–35]

This reorganization/reaction phenomenon of Si at the Ni (111), followed by a partial dissolution process (up to the superstructure), seems to deeply mark the topography of the surface. Indeed, filled state STM images [Fig. 4(a)] recorded after the dissolution process at 400 °C (annealing time 45 min) and the formation of the $(\sqrt{3}\times\sqrt{3})R30^\circ$ superstructure (180×180 nm^2) appear very corrugated with many holes

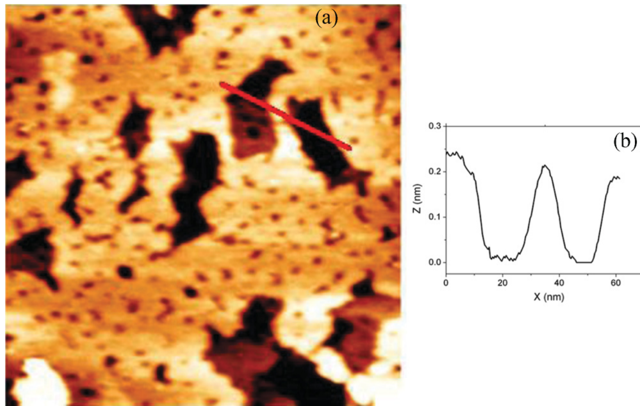

FIG. 4. (Color online) (a) STM image of the Ni (111) surface covered by 1 Si ML after annealing at 400 °C (imaging conditions: 0.9 V sample bias and 1.2 nA tunnel current); (b) line scan showing the depth holes.

(small and large). The depth profile reported in Fig. 4(b) gives the average depth of these holes, which is approximately equal to 0.2 nm. These holes, not present on the clean Ni (111) surface (not shown here), are likely the mark of the first steps of the Si deposition process followed by dissolution of the 3D silicide islands.

A magnification taken on a flat part of Fig. 4 shows the $(\sqrt{3} \times \sqrt{3})R30^{\circ}$ superstructure atomically resolved (filled state STM image reported on Fig. 5).

On this STM image the average distance separating two successive rows in the periodic arrangement is about 0.43 nm, which corresponds to $\sqrt{3}a_{\mathrm{Ni}}$ (with $a_{\mathrm{Ni}} = 0.249$ nm the distance between first nearest neighbors on the Ni (111) surface). On these rows, the corrugation amplitude is close to 0.02 ± 0.01 nm as shown by the line scan reported in Fig. 5. This weak corrugation suggests that the atoms inducing the $(\sqrt{3} \times \sqrt{3})R30^{\circ}$ superstructure are inserted in the plane of the topmost layer forming a 2D surface alloy (2D silicide) as is generally observed in similar systems.[36,37]

Based only on the STM image, it is impossible to say if the 2D silicide is Ni_2Si or $NiSi_2$. However, dissolution kinetics (isochronal and isothermal) monitored by AES (Figs. 1 and 3) show that the sharper $(\sqrt{3} \times \sqrt{3})R30^{\circ}$ LEED pattern is obtained after dissolution of about two thirds of a Si ML, which is in favor of a Ni-rich compound, i.e., Ni_2Si.

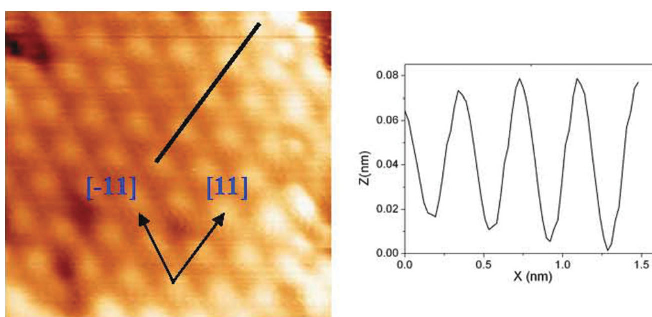

FIG. 5. (Color online) A typical filled-states STM image of the Ni (111) surface showing the $(\sqrt{3} \times \sqrt{3})R30^{\circ}$ superstructure obtained after annealing at 400 °C for 10 min of 1 Si ML (0.5 V, 1.4 nA).

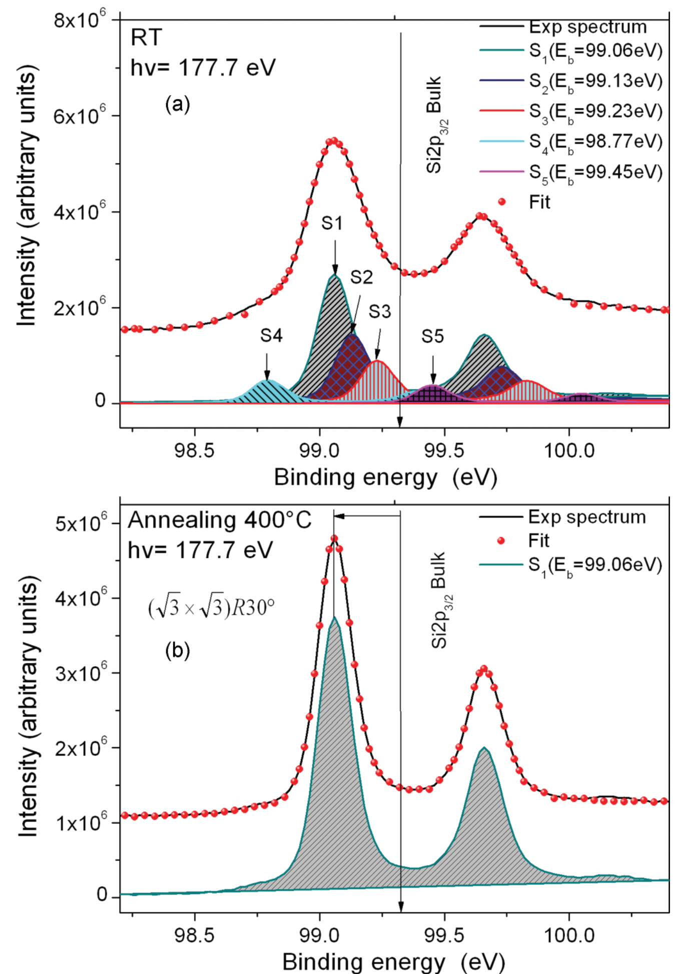

FIG. 6. (Color online) Si_{2p} core levels (a) after deposition at RT of 1 ML of Si onto Ni(111); (b) after annealing at 400 °C (45 min).

Finally, we have performed at RT high-resolution photoelectron spectroscopy (HR-PES) measurements of the Si_{2p} core levels. Figures 6(a) and 6(b) present two photoemission spectra of the Si_{2p} core levels, recorded, respectively, just after deposition at RT of 1 Si ML onto a clean Ni(111) substrate and after annealing at 400 °C for 10 min (with the superstructure checked by LEED). Both spectra are obtained with the same energy of photons ($E = 177.7$ eV) and the same geometry (emission angle 45°, acceptance angle 16°). The binding energies are referenced with regard to the Fermi level and the peaks fitted with a Donia-Sunjic[38] peak line shape and a Shirley-type[39] background. The best fit is obtained with the following parameters: a Gaussian and a Lorentzian with a FWHM, respectively, of 0.15 eV and 0.08 eV; a spin-orbit splitting of 0.60 eV; a branching ratio of 0.5; and an asymmetry parameter of 0.05.

With these parameters, the peak after deposition of 1 Si ML appears to be composed of five components: an intense component S_1 (99.06 eV), and four other components: S_2 (99.13 eV), S_3 (99.23 eV), S_4 (98.77 eV), and S_5 (99.45 eV), showing the coexistence of different chemical environments of Si atoms. The S_1, S_2, S_3, S_4, S_5, components are indicated for each spectrum at the bottom of Fig. 6(a). For comparison,

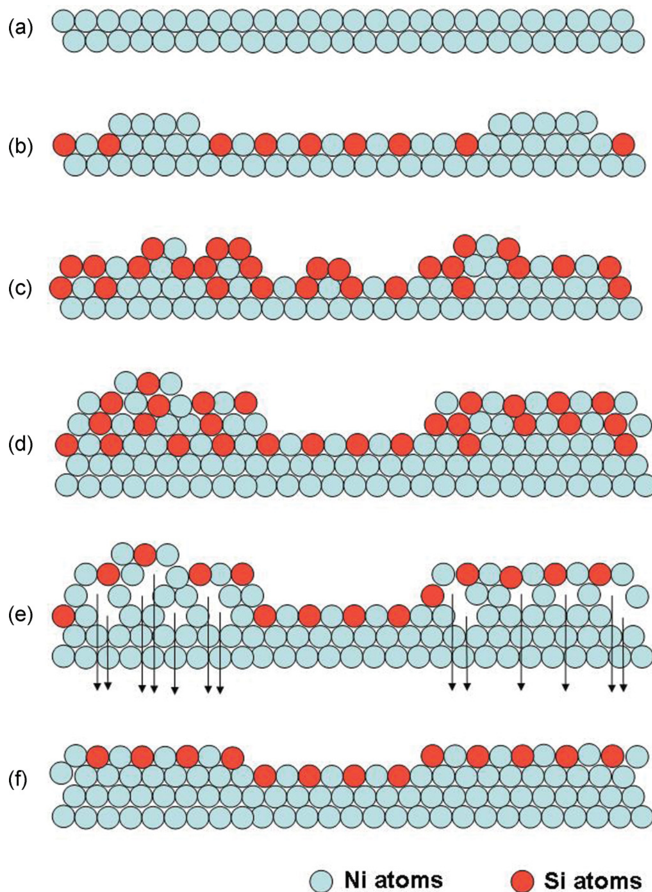

FIG. 7. (Color online) Side view schematic atomic model suggesting the scenario observed during deposition and dissolution of about 1 Si ML on Ni(111); (a) large terrace of bare Ni(111); (b) first step of the Si deposition (formation of Ni terraces due to Si atoms insertion process); (c) after deposition of about 1 Si ML; (d) domain I observed by Auger spectroscopy during isochronal and isothermal annealing: formation of 3D silicide islands; (e) domain II: dissolution in the bulk of the Si atoms not located in the topmost surface layer due to the segregation phenomenon (i.e., dissolution of the 3D silicide islands); (f) domain III: blockage of the dissolution process on a 2D silicide resulting in a surface roughness.

the binding energy position of the $Si_{2p3/2}$ peak measured on a Si (111) (bulk peak) in our experimental configuration is also indicated by a solid line ($E_b = 99.3$ eV).

The S_5 component ($El = 99.45$ eV) close to that of the Si bulk (99.3 eV) can be attributed to the Si atoms being bound to other Si atoms and at the topmost surface layer. The (S_1, S_2, S_3, S_4) components are more or less strongly shifted in energy toward the lower binding energy. This reflects an electron transfer between silicon and nickel and suggests that these Si atoms are in strong interaction with the nickel atoms; each component could be a signature of the number of Ni atoms, and the more a silicon atom is surrounded by nickel atoms, the more its core level will be shifted toward lower binding energy. This also shows that the first Si atoms instantaneously react with the Ni substrate to form intermetallic compounds unstructured or ordered at up to a short distance, and thus not observable by LEED.

Using the same set of parameters, the Si_{2p} core levels recorded after annealing at 400 °C can be fitted with only one doublet as shown in Fig. 6(b). Existence of only one component indicates that the Si atoms are in a single chemical environment, i.e., every Si atom in the surface layer is surrounded by the same number of Ni atoms forming the ordered $(\sqrt{3} \times \sqrt{3})R30^\circ$ surface alloy observed by LEED. On the topmost surface layer, this corresponds to the 2D silicide Ni_2Si. Note that this component is already present at RT (and is the most intense) just after silicon deposition [Fig. 5(a)]. This shows the natural tendency of the system to form locally a 2D silicide with a composition close to Ni_2Si. Note also that this Si_{2p} core level spectrum presents a large asymmetry parameter (0.05). This asymmetry is the signature of a high metallic character of silicon on nickel since it is associated to a high density of states at the Fermi level. This metallic character of the silicon atoms can explain the corrugation observed on the STM images (Fig. 5), showing mainly the silicon atoms forming the $(\sqrt{3} \times \sqrt{3})R30^\circ$ superstructure.

One can note that the total integrated intensity, the Si_{2p} peak decreases of about two thirds after the annealing treatment [the total area of the Si_{2p} components decreases from 3.8 arbitrary units (arb. units), just after deposition, to 1.15 arb. units after annealing], is in very good agreement with the previous AES data presented in the first section (Results and Discussions) and confirms the chemical composition of the 2D silicide (Ni_2Si).

Finally, from all results (Auger, LEED, STM, and PES), we can propose the following scheme (Fig. 7):

(i) Most of the silicon atoms (for a monolayer deposit) react instantaneously during deposition with the nickel substrate to form unstructured intermetallic compounds or ordered compounds at short distance as schematically shown in Figs. 7(b) and 7(c) (PES + LEED).

(ii) In domain I (observed by AES during isochronal and isothermal dissolution), 3D silicide islands are formed in equilibrium on a 2D surface silicide [Fig. 7(d)].

(iii) In domain II, the 3D silicide islands dissolve (diffusion of Si atoms at the interface between the islands and the substrate) until a 2D silicide is formed. The surface roughness observed by STM (about 0.2 nm, Fig. 4) could be the signature of insertion of Si atoms in the topmost Ni surface layer [during the first step of deposition as schematically shown in Fig. 7(b)] followed by the dissolution process of the 3D islands [Fig. 7(e)].

(iv) In domain III, the dissolution kinetics is blocked on a 2D silicide as shown by AES, PES, LEED, and STM [Fig. 7(f)].

IV. CONCLUSIONS

We have studied by AES-LEED, HR-PES, and STM the temperature effect on 1 ML of Si deposited onto Ni (111). The Si deposition at RT leads to the formation of a disordered 2D and/or 3D intermetallic compound. The main effect of the isothermal or isochronal annealing is to dissolve the excess of Si in the bulk and to form a stable and well ordered 2D Ni_2Si intermetallic compound giving rise to a $(\sqrt{3} \times \sqrt{3})R30^\circ$ superstructure. In this surface alloy, Si is found to be inserted in the topmost surface layer with a strong metallic character. This surface alloy shows a stability with temperature up to at least 400 °C.

[*]Corresponding author: LALMI@synchrotron-soleil.fr

[1]K. Kataoka, K. Hattori, Y. Miyatake, and H. Daimon, Phys. Rev. B **74**, 155406 (2006).
[2]D. Grozea, E. Bengu, and L. D. Marks, Surf. Sci. **461**, 23 (2000).
[3]Z. Q. Zou, D. Wang, J. J. Sun, and J. M. Liang, J. Appl. Phys. **107**, 014302 (2010).
[4]P. Höpfner, M. Wisniewski, F. Sandrock, J. Schäfer, and R. Claessen, Phys. Rev. B **82**, 075431 (2010).
[5]L. Casalis, A. Citti, R. Rosei, and M. Kiskinova, Phys. Rev. B **51**, 1954 (1995).
[6]P. A. Bennett and H von Känel, J. Phys. D: Appl. Phys. **32**, 71 (1999).
[7]A. Ouerghi, J. Peneluas, C. Andreazza-Vignolle, P. Andreazza, N. Bouet, and H. Estrade-Szwarckopf, J. Appl. Phys. **100**, 124310 (2006).
[8]R. J. Phaneuf, Y. Hong, S. Horch, and P. A. Bennett, Phys. Rev. Lett. **78**, 4605 (1997).
[9]A. E. Dolbak, B. Z. Olshanetsky, S. I. Stenin, S. A. Teys, and T. A. Gavrilova, Surf. Sci. **247**, 32 (1991).
[10]R. J. Phaneuf and P. A. Bennett, Surf. Rev. Lett. **5**, 1179 (1988).
[11]H. von Kanel, Mater. Sci. Rep. **8**, 193 (1992).
[12]Y. Khang, S. J. Kahng, K. M. Mang, D. Jeon, J. H. Lee, Y. N. Kim, and Y. Kuk, J. Vac. Sci. Technol. B **12**, 2094 (1994).
[13]J. M. Gibson and J. L. Batstone, Surf. Sci. **208**, 317 (1989).
[14]R. J. Wilson and S. Chiang, Phys. Rev. Lett. **58**, 2575 (1987).
[15]G. Kinoda and K. Ogawa, Surf. Sci. **461**, 67 (2000).
[16]L. Gregoratti, S. Günther, J. Kovaĉ, M. Marsi, R. J. Phaneuf, and M. Kiskinova, Phys. Rev. B **59**, 2018 (1999).
[17]T. Yao, S. Shinabe, and M. Yoshimura, Appl. Surf. Sci. **104/105**, 1029 (1996).
[18]S. A. Parikh, M. Y. Lee, and P. A. Bennett, Surf. Sci. **356**, 53 (1996).
[19]P. A. Bennett, M. Y. Lee, S. A. Parikh, K. Wurm, and R. J. Phaneuf, J. Vac. Sci. Technol. A **13**, 1728 (1995).
[20]L. Gregoratti, S. Günther, J. Kovac, M. Marsi, and M. Kiskinova, Surf. Sci. **439**, 120 (1999).
[21]Y. Khang and Y. Kuk, Phys. Rev. B **53**, 10775 (1996).
[22]M. Yoshimura, I. Ono, and K. Ueda, Appl. Surf. Sci. A **130**, 276 (1998).
[23]D. Loretto, J. M. Gibson, and S. M. Yalisove, Phys. Rev. Lett. **63**, 298 (1989).
[24]U. Falke, A. Bleloch, M. Falke, and S. Teichert, Phys. Rev. Lett. **92**, 116103 (2004).
[25]P. Nash and A. Nash, Bull. Alloy Phase Diagrams **8**, 1 (1987).
[26]B. Lalmi, C. Girardeaux, A. Portavoce, J. Bernardini, and B. Aufray, J. Nanosci. Nanotechnol. **9**, 4311 (2009).
[27]B. Lalmi, Ph.D. thesis, Université Paul Cézanne-Marseille III, Aix-en-Provence, France, 2009.
[28]A. R. Miedema and J. W. F. Dorleijn, Surf. Sci. **95**, 447 (1980).
[29]S. Hofmann and J. Erlewein, Scr. Metal. **10**, 857 (1976).
[30]M. Lagües and J. L. Domange, Surf. Sci. **47**, 77 (1975).
[31]J. Eugène, B. Aufray, and F. Cabane, Surf. Sci. **241**, 1 (1991).
[32]R. A. Swalin, A. Martin, and R. Olson, Trans. AIME **209**, 936 (1957).
[33]H. Giordano, J. P. Biberian, and B. Aufray, Surf. Sci. **313**, 266 (1994).
[34]H. Giordano and B. Aufray, Surf. Sci. **307–309**, 816 (1994).
[35]F. Abel, C. Cohen, J. A. Davis, J. Moulin, and D. Schmaus, Appl. Surf. Sci. **44**, 17 (1990).
[36]J. A. Martin-Gago, R. Fasel, J. Hayoz, R. G. Agostino, D. Naumovic, P. Aebi, and L. Schlapbach, Phys. Rev. B **55**, 12896 (1997).
[37]C. Polop, C. Rojas, J. A. Martin-Gago, R. Fasel, J. Hayoz, D. Naumovic, and P. Aebi, Phys. Rev. B **63**, 115414 (2001).
[38]S. Doniach and M. Sunjic, J. Phys. C **3**, 285 (1970).
[39]D. A. Shirley, Phys. Rev. B **5**, 4709 (1972).